Journal of Biomolecular NMR, 2 (1992) 257–274
ESCOM

J-Bio NMR 056

Precise vicinal coupling constants $^3J_{HN\alpha}$ in proteins from nonlinear fits of J-modulated [^{15}N,^1H]-COSY experiments

Martin Billeter, Dario Neri, Gottfried Otting, Yan Qiu Qian and Kurt Wüthrich*

Institut für Molekularbiologie und Biophysik, Eidgenössische Technische Hochschule-Hönggerberg, CH-8093 Zürich, Switzerland

Received 6 November 1991
Accepted 18 December 1991

Keywords: Vicinal spin-spin coupling constants; J-modulated [^{15}N,^1H]-COSY; Nonlinear fit of J-modulation; Protein conformation; NMR structure of proteins

SUMMARY

Improved experimental schemes for the recently introduced J-modulated [^{15}N,^1H]-correlation experiment for measurements of the homonuclear amide proton-C^α proton vicinal coupling constants, $^3J_{HN\alpha}$, in uniformly ^{15}N-labeled proteins are described, and a nonlinear fit procedure is presented for quantitative evaluation of $^3J_{HN\alpha}$. The method was first tested with the N-terminal DNA-binding domain of the 434 repressor (M = 7.3 kDa), where at 13 C precise values of $^3J_{HN\alpha}$ in the range 2.0–9.5 Hz were obtained for all residues with resolved ^{15}N-^1H cross peaks. It was then applied to the *Antennapedia* homeodomain complexed to a synthetic 14-base pair DNA fragment (molecular weight of the complex ~ 18 kDa). The $^3J_{HN\alpha}$ values measured were found to be in excellent agreement with those predicted from the secondary structure of this protein in the complex.

INTRODUCTION

After a decade dominated by measurements of NOEs leading to complete protein structure determination in solution (Wüthrich, 1986, 1990), we presently witness a revival of interest in coupling constants. Based on Karplus-type relations (Karplus, 1959, 1963; Bystrov, 1976) vicinal coupling constants provide essential supplementary information on local conformation and conformational equilibria (Nagayama and Wüthrich, 1981), and support the determination of individual assignments for pairs of diastereotopic ligands (Arseniev et al., 1988; Güntert et al., 1989).

* To whom correspondence should be addressed.

Abbreviations and symbols: NOE, nuclear Overhauser effect; COSY, two-dimensional correlated spectroscopy; $^3J_{HN\alpha}$ or J, homonuclear vicinal amide proton-C^α proton coupling constant; 434 repressor(1-69), N-terminal DNA-binding domain of the 434 repressor comprising 69 residues.

0925-2738/$ 5.00

Motivated by this renewed interest, numerous novel NMR experiments for studies of spin-spin coupling constants have recently been proposed, in particular also for measurements of amide proton-C^{α} proton coupling constants, $^{3}J_{HN\alpha}$ (e.g., Kay et al., 1989; Montelione and Wagner, 1989; Kim and Prestegard, 1989; Kay and Bax, 1990; Ludvigsen et al., 1991; Wagner et al., 1991). *J-modulated [^{15}N,^{1}H]-COSY* (Neri et al., 1990) is also one of the experiments proposed for this purpose, which has so far been used for qualitative measurements of $^{3}J_{HN\alpha}$ in uniformly ^{15}N-enriched proteins. The present article describes a procedure that permits quantitative measurements of the vicinal coupling constants $^{3}J_{HN\alpha}$ even in relatively large molecular species, using a nonlinear fit of the [^{15}N,^{1}H]-COSY cross-peak volumes to the expected damped oscillations of the coherence during a delay before signal acquisition.

The vicinal coupling constants $^{3}J_{HN\alpha}$ have long had a special role because they have often been the most readily accessible NMR parameters that could be related to polypeptide backbone conformation. Special care has therefore been taken to establish empirical calibrations of the Karplus-type equations for $^{3}J_{HN\alpha}$ (Bystrov, 1976; De Marco et al., 1978), and recognition of specific patterns of $^{3}J_{HN\alpha}$ values along the amino acid sequence has been applied for the identification of

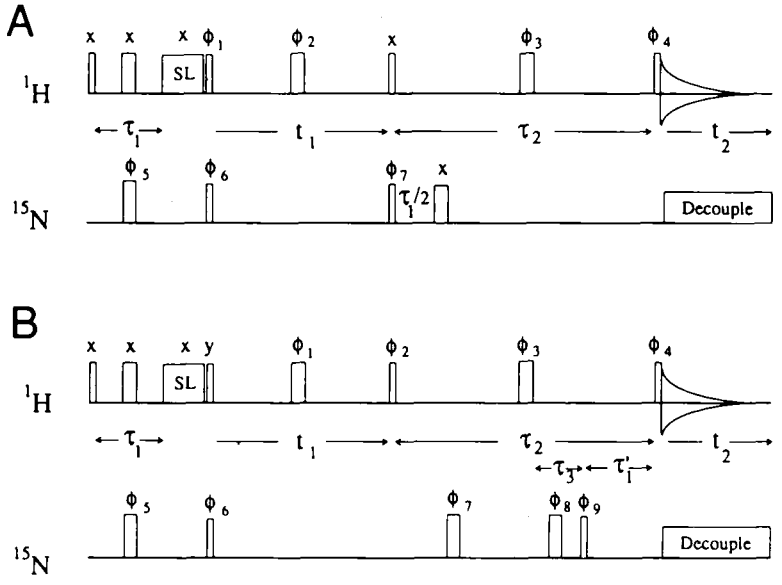

Fig. 1. Experimental schemes for measurements of $^{3}J_{HN\alpha}$ with J-modulated [^{15}N,^{1}H]-COSY. Narrow vertical bars indicate $\pi/2$ pulses, wide bars are π pulses; SL indicates a spin-lock purge pulse of 2 ms length (Otting and Wüthrich, 1988). The delays τ_1 and $\tau'_1 = \tau_1$ are tuned to $1/2\ ^{1}J(^{15}N,^{1}H)$. τ_2 is a variable delay; for measurements of $^{3}J_{HN\alpha}$ a series of spectra with different τ_2 values is recorded. (A) Previously used scheme (Neri et al., 1990) supplemented with a refocusing $(\pi)_x(^{15}N)$ pulse and heteronuclear decoupling in t_2. (B) Pulse sequence recommended for studies of bigger-sized proteins. $\tau_3 = \frac{\tau_2}{2} - \tau'_1 - \tau(\Phi_9) - \frac{\tau(\Phi_3)}{2}$, where the $\tau(\Phi_i)$s are the lengths of the pulses with phase Φ_i. All π-pulses are centrally located in the time period between the immediately preceding and following pulses on either channel, except for the pulse $\pi_{\Phi 3}(^{1}H)$, which is in the centre of τ_2. Phase cycles are described in Table 1. Water suppression is achieved with the 2 ms spin-lock pulse (Messerle et al., 1989). Alternatively, the schemes may be preceded by selective irradiation of the water signal, or the two solvent suppression techniques may be combined.

regular secondary structures in proteins (Pardi et al., 1984). However, it has also been found that measurements of $^3J_{HN\alpha}$ in homonuclear ^1H NMR spectra can be beset with systematic errors once the natural line widths are comparable to the J values (Neuhaus et al., 1985). In this paper we show that J-modulated [^{15}N,^1H]-COSY enables reliable measurements of $^3J_{HN\alpha}$ also under these limiting conditions. The method is straightforward in its practical application, and since uniform ^{15}N-labeling of proteins is becoming more and more common (McIntosh and Dahlquist, 1990), it should be quite widely applicable.

THEORY AND COMPUTATIONAL METHODS

In J-modulated [^{15}N,^1H]-COSY (Neri et al., 1990) one observes the modulation of the amide proton magnetization by the scalar coupling $^3J_{HN\alpha}$ during a delay τ_2 at the end of heteronuclear correlation experiments (Bodenhausen and Ruben, 1980). In this section we describe improved J-modulated heteronuclear COSY experiments that are suitable for studies of $^3J_{HN\alpha}$ in proteins of different sizes, the general strategy used for the data processing, and a nonlinear fit procedure that enables a quantitative determination of $^3J_{HN\alpha}$. Experimental details are given in the Results section, primarily in the figure captions.

Experimental schemes for J-modulated [^{15}N,^1H]-COSY

Figure 1 and Table 1 present two J-modulated [^{15}N,^1H]-COSY experiments. These experiments rely on the observation of the amide proton resonances, so that the measurements have to be performed in H_2O solution with the use of a suitable solvent suppression scheme. In the experimental schemes of Fig. 1 the water signal is suppressed by a spin-lock pulse, SL_x (Messerle et al., 1990). Alternatively, one could use presaturation by selective irradiation at the water frequency before each scan, provided that the loss in sensitivity arising from saturation transfer to the amide protons is acceptable under the experimental conditions used.

The experimental scheme of Fig. 1A is the previously used experiment (Neri et al., 1990) supple-

TABLE 1
PHASE CYCLES FOR THE EXPERIMENTAL SCHEMES A AND B OF FIG. 1

	A	B
Φ_1	$(y)_{32}(-y)_{32}$	$(x,-x)_{128}$
Φ_2	$[(x)_2(-x)_2]_{16}$	$[(x)_{32}(-x)_{32}]_4$
Φ_3	$[(x)_4(-x)_4(y)_4(-y)_4]_4$	$[(x)_2(-x)_2(y)_2(-y)_2]_{32}$
Φ_4	$[(x)_{16}(-x)_{16}]_2$	$[(x)_{16}(-x)_{16}]_8$
Φ_5	$(x)_{64}$[a]	$(x)_{256}$[a]
Φ_6	$(x)_{32}(-x)_{32}$[a]	$(x)_{256}$[a]
Φ_7	$(x,-x)_{32}$	$[(x)_{64}(-x)_{64}]_2$
Φ_8		$(x)_{128}(-x)_{128}$
Φ_9		$[(x)_8(-x)_8]_{16}$
Receiver	$[(x,-x)_4(-x,x)_4]_4$	$\{[(x)_4(-x)_8(x)_8(-x)_8(x)_4][(-x)_4(x)_8(-x)_8(x)_8(-x)_4]\}_4$

[a] Pulses that were subjected to TPPI for quadrature detection (Marion and Wüthrich, 1983).

mented with a refocusing $\pi(^{15}N)$ pulse and heteronuclear decoupling during t_2 using a WALTZ-16 decoupling sequence with suppression of cycling sidebands (Shaka et al., 1986). Decoupling during t_1 is achieved with a proton π-pulse with phase Φ_2, which refocuses the heteronuclear antiphase magnetization. The phase cycles are listed in Table 1. In J-modulated [^{15}N,^1H]-COSY experiments, the quantity of interest is the variation of intensity and sign of the cross peaks in the [^{15}N,^1H]-plane as a function of the delay time τ_2. The delay time τ_2^0 at which a cross peak changes its sign is approximately related to the $^3J_{HN\alpha}$ coupling constant of the observed residue by the relation

$$\tau_2^0 = \frac{1}{2\,{}^3J_{HN\alpha}} \tag{1}$$

In earlier applications of J-modulated [^{15}N,^1H]-COSY, Eq. 1 was used to calculate the $^3J_{HN\alpha}$'s from τ_2^0-values. These were estimated from a series of measurements performed with different delay times τ_2, checking for which τ_2 value the sign of a given cross peak is inverted (Neri et al., 1990).

With 64 steps the experimental scheme of Fig. 1A has a shorter phase cycle than the scheme of Fig. 1B. It is therefore best suited for small proteins with inherently good signal-to-noise ratios. The scheme B offers more favourable spin relaxation behaviour, which is crucial for work with bigger molecules with rapid T_2 relaxation, since it selects transverse heteronuclear two-spin coherence at the start of the J-modulation period τ_2. It is the pulse sequence of choice for larger proteins.

A product operator description (Sørensen et al., 1983) identifies the terms required for the precise evaluation of the coupling constants $^3J_{HN\alpha}$, and leads to the origin of the different relaxation rates observed in the two experiments of Fig. 1. H^N, H^α and N denote the spin operators of the amide proton, the C^α-proton and the ^{15}N nucleus, respectively. Starting from equilibrium magnetization, H_z^N, and with $\tau_1 = 1/2^1J(^{15}N,^1H)$, we have the following terms at the beginning of the spin-lock pulse, SL_x:

$$2H_x^N N_z \cos(\pi J\tau_1) + 4H_y^N H_z^\alpha N_z \sin(\pi J\tau_1) \tag{2}$$

If terms cancelled by the phase cycling are omitted, the first term of Eq. 2 evolves as

$$2H_x^N N_z \xrightarrow{SL_x(^1H)} 2H_x^N N_z \xrightarrow{\left(\frac{\pi}{2}\right)_y(^1H),\left(\frac{\pi}{2}\right)_x(^{15}N)} -2H_z^N N_y$$

$$\xrightarrow{t_1/2\text{-}\pi(^1H)_x\text{-}t_1/2} -2H_z^N N_y \cos(\Omega_N t_1) \xrightarrow{\left(\frac{\pi}{2}\right)_x(^1H)} 2H_y^N N_y \cos(\Omega_N t_1) \tag{3}$$

where Ω_N is the angular frequency of the ^{15}N spin relative to the ^{15}N carrier frequency. In the experimental scheme of Fig. 1A the additional pulse $\left(\frac{\pi}{2}\right)_{\Phi_3}(^{15}N)$ in the last step of Eq. 3 converts the

heteronuclear two-spin coherence $2H_y^N N_y$ immediately into single-quantum magnetization $2H_y^N N_z$, which evolves during the delay τ_2 into H_x^N magnetization with a $\cos(\pi J\tau_2)$ dependence and relaxes as single-quantum coherence throughout the delay τ_2. The $\left(\frac{\pi}{2}\right)_{\Phi_4}(^1H)$ pulse immediately before detection purges any amide proton magnetization in antiphase with respect to the α-proton by converting it into α-proton magnetization. In the experimental scheme of Fig. 1B the coherence $2H_y^N N_y$ evolves also with $\cos(\pi J\tau_2)$ during τ_2 but relaxes as multiple-quantum coherence during the interval $(\tau_2-\tau_1')$. This term is converted into $2H_y^N N_z$ magnetization only by the $\left(\frac{\pi}{2}\right)_{\Phi_5}(^{15}N)$ pulse near the end of the delay τ_2, before the heteronuclear antiphase magnetization is refocused during τ_1'.

The second term of Eq. 2 leads to observable magnetization only if the spin-lock pulse SL_x is used (Fig. 1), which converts this term according to

$$4H_y^N H_z^\alpha N_z \xrightarrow{SL_x(^1H)} -4H_z^N H_y^\alpha N_z \sin^2\beta + ... \tag{4}$$

where further, irrelevant terms were omitted and β is the effective flip angle of the spin-lock pulse. Because of virtually complete averaging of the flip angles over the sample due to the radiofrequency inhomogeneity of the spin-lock pulse, the term $\sin^2\beta$ is averaged to 0.5. The coherence $-2H_z^N H_y^\alpha N_z$ is then further converted as described by Eq. 5:

$$-2H_z^N H_y^\alpha N_z \xrightarrow{\left(\frac{\pi}{2}\right)_y(^1H),\left(\frac{\pi}{2}\right)_x(^{15}N)} 2H_x^N H_y^\alpha N_y$$

$$\xrightarrow{t_1/2-\pi(^1H)_x-t_1/2} -2H_x^N H_y^\alpha N_y \cos(\Omega_N t_1) \xrightarrow{\left(\frac{\pi}{2}\right)_x(^1H)} -2H_x^N H_z^\alpha N_y \cos(\Omega_N t_1) \tag{5}$$

During τ_2 the final product operator in Eq. 5 evolves into H_x^N magnetization with a $\sin(\pi J\tau_2)$ dependence. Therefore, if one collects all the trigonometric terms containing J, the volume of the ^{15}N-amide proton cross peaks, V, is modulated as described by Eq. 6.

$$V \propto [\cos(\pi J\tau_1)\cos(\pi J\tau_2) - 0.5\sin(\pi J\tau_1)\sin(\pi J\tau_2)] \tag{6}$$

While the t_1-evolution of the term $2H_z^N N_y$ of Eq. 3 results in an absorption-mode singlet in the ω_1-dimension, the term $2H_x^N H_y^\alpha N_y$ of Eq. 5 contributes a component to the cross peak which has an absorption-mode, in-phase multiplet fine structure in the ω_1-dimension due to $^3J_{\alpha\beta}$ scalar couplings. In writing Eq. 6 it is assumed that the cross peaks are integrated over their entire width in the ω_1-dimension.

In special situations, where the improved peak separation of a 2D spectrum is not needed, 1D variants of the experiments of Fig. 1 may be preferable. An illustration is provided by the recently

described study of a complex of the ^{15}N-labeled cyclic undecapeptide cyclosporin A with unlabeled cyclophilin (molecular weight of the complex: 18.9 kDa) (Weber et al., 1991), where the $^3J_{HN\alpha}$ values for the 4 nonmethylated amide groups of cyclosporin A were determined with a 1D variant of the experiment of Fig. 1A. 1D versions of the 2D experiments of Fig. 1 are obtained by elimination of the sequence $\left(\frac{\pi}{2}\right)(^1H)$-$t_1/2$-$\pi(^1H)$-$t_1/2$-$\left(\frac{\pi}{2}\right)(^1H)$ from the respective experimental schemes. Due to the omission of Φ_1 and Φ_2, the length of the phase cycles is reduced by a factor 4. Basically, with the phase cycling used (Table 1) the 1D versions are ^{1}H NMR experiments containing a pulse sequence corresponding to a ^{15}N half filter element of the type $\tau_1/2$-$\pi_x(^1H),\pi_{\Phi_5}(^{15}N)$-$\tau_1/2$-$SL_x(^1H)$, $\left(\frac{\pi}{2}\right)_x(^{15}N)$-$\left(\frac{\pi}{2}\right)_{\pm x}(^{15}N)$ (Otting and Wüthrich, 1990). The result is a difference spectrum which contains only the resonances of ^{15}N-bound protons.

Data processing and spectral analysis

In the [^{15}N,^{1}H]-COSY spectrum of a protein with 100 amino acid residues, about 100 ^{15}N-^{1}H cross peaks must be identified and integrated for each value of τ_2, so that of the order of 1000 peaks need to be evaluated for a $^3J_{HN\alpha}$ determination. This process can nowadays be largely automated, provided that care is taken to identically record and process the data at different τ_2 values. Based on the chemical shifts obtained previously from the sequence-specific resonance assignments (Wüthrich, 1986), we used the program EASY (Eccles et al., 1991) for picking, assignment and integration of the cross peaks. After interactive selection of integration areas for each peak in the first spectrum, EASY automatically integrated the same areas in all the spectra and produced lists of peak volumes suitable for the fitting program.

Quantitative determination of $^3J_{HN\alpha}$ from J-modulated [^{15}N,^{1}H]-COSY data

From the above product operator analysis of J-modulated [^{15}N,^{1}H]-COSY it is clear that in addition to the modulation of the coherence by $^3J_{HN\alpha}$ during τ_2 as $\cos(\pi J\tau_2)$, a quantitative analysis of the experimental data must also consider the evolution of the amide proton magnetization under J during the short delay τ_1, as well as the nuclear spin relaxation during τ_2. This is achieved through fitting of the expression (7) to the experimental dependence of the cross-peak volumes on τ_2 (see Fig. 3).

$$\bar{V}(\tau_2) = A\cdot[\cos(\pi J\tau_1)\cos(\pi J\tau_2) - 0.5\sin(\pi J\tau_1)\sin(\pi J\tau_2)]\cdot e^{(-\tau_2/T_2')} \qquad (7)$$

where $\bar{V}(\tau_2)$ is the cross-peak volume as a function of the delay time τ_2, A the cross-peak volume at $\tau_2 = 0$, J the coupling constant $^3J_{HN\alpha}$, and T_2' the apparent transverse spin relaxation time. In the experiment of Fig. 1B the effective relaxation rate for the coherence evolving during $\tau_2 - \tau_1'$ is given by the arithmetic mean of the relaxation rates for heteronuclear zero- and double-quantum coherence, because each π-pulse interconverts zero-quantum coherence into double-quantum coherence, and vice versa. Further relaxation of the single-quantum coherence during the constant delay τ_1' contributes a constant factor to the overall relaxation during τ_2, which is therefore well approximated by the single relaxation time T_2'.

For the assessment of the uncertainty in the experimental cross-peak volumes, one has to ac-

count for the fact that even very small volumes have a finite error arising from the random noise, and that some error components increase with increasing volumes, e.g., side lobes of cross peaks, or t_1-noise. The most simple model consistent with these requirements is a linear error dependence on the cross-peak volumes with a nonvanishing error value for zero volumes. In our implementation of the fitting procedure, the errors attributed both to zero volume and to the largest peak in the spectrum recorded for the shortest τ_2-value are selected by the user as percentage values of the volume of this largest peak. For cross-peak volumes intermediate between these two extreme values, the error is then obtained by linear interpolation. These somewhat arbitrary error estimates are not critical, since variation by as much as a factor 2 did not noticeably affect the J values obtained.

Initial estimates for the fit parameters A, J and T'_2 in Eq. 7 were obtained as follows: an approximate value of τ_2^i (Eq. 1) was obtained by linear interpolation between the two experimental points along τ_2 for which the last positive and the first negative peak volumes were observed, and the start value of J was then obtained with Eq. 1. When no zero passage could be observed, the largest τ_2 value for which a spectrum had been recorded was used in the place of τ_2^i. The start value for J was then inserted into Eq. 7, and initial values for A and T'_2 were obtained by a linear fit. The Levenberg–Marquardt algorithm (e.g., Press et al., 1986) was used to minimize the expression

$$\chi^2 = \sum_{i=1}^{n} [V(\tau_2^i) - \bar{V}(\tau_2^i)]^2 \tag{8}$$

where the summation is over all n experimental values of τ_2. χ^2_{min} is thus the sum of the squares of the deviations between the measured cross-peak volumes, $V(\tau_2)$, and the corresponding values $\bar{V}(\tau_2)$ calculated with Eq. 7 after an optimal fit of A, J and T'_2 against $V(\tau_2)$.

For the assessment of the error range to be attributed to the J values obtained with the above procedures, one has to allow for the fact that the errors in J do not depend solely on the uncertainties in the experimental cross-peak volumes, but that other aspects of the experiment used and its interpretation are also of importance, e.g., the choice of the number of different delay times τ_2, and the validity of the approximation that the overall relaxation can be described by a single exponential function. Therefore, the error in J cannot be related directly to the errors in the cross-peak volumes. In principle, the Levenberg–Marquardt algorithm provides an error estimate based on the quality of the fit according to Eqs. 7 and 8, thus considering all experimental aspects of the determination of J. However, since this estimate is calculated from the curvature of the plot of χ^2 vs. J, it describes only the local behaviour near the final, optimal fit values for J, A and T'_2, and it usually yields very small error ranges. A grid search, where $^3J_{HN\alpha}$ was systematically varied in steps of 0.1 Hz over the range 0–11 Hz and the parameters A and T'_2 were fitted with Eq. 7 for minimal χ^2 with each J value, showed that the distribution of χ^2 values is not necessarily symmetric relative to the optimal fit value for J at χ^2_{min}. In practice, the dependence of χ^2 on $^3J_{HN\alpha}$ obtained from such a grid search is therefore used to characterize the precision with which the coupling constants were measured, using asymmetric lower and upper limits, J_l and J_u, for the measured $^3J_{HN\alpha}$ values. These limits are given by the two values of J where the $\chi^2(J)$ curves have a (somewhat arbitrarily) predetermined value in the range between $2\chi^2_{min}$ and $5\chi^2_{min}$.

RESULTS

This section starts with an illustration of the impact of the different relaxation mechanisms effective in the experiments A and B in Fig. 1. To illustrate the use of the presently introduced method for the determination of $^3J_{HN\alpha}$ under conditions where the application of other techniques for measurements of these coupling constants is limited by line broadening, we then show data for a small protein recorded at low temperature, and for a protein bound to DNA in a complex of molecular weight 18 000. In both applications we assumed that the error for experimental determination of zero volumes is 0.5% of the largest cross-peak volume observed in the spectrum recorded with the shortest delay τ_2. For both systems, this value is larger than the volumes obtained when integrating the random noise in spectral areas of similar size as the areas around the cross peaks used for the peak integration. The error attributed to the largest cross peak was taken as 10% of its volume.

Impact of different relaxation regimes

The impact of the different relaxation regimes encountered when using either experiment A or experiment B in Fig. 1 is nicely illustrated with the experiment with ^{15}N-labeled 434 repressor(1–69) at 13°C shown in Fig. 2. The two spectra were recorded, respectively, using the experiment of Fig. 1A without ^{15}N refocusing pulse during τ_2 and without heteronuclear decoupling during τ_2 (Neri et al., 1990), and using the experiment of Fig. 1B without refocusing (i.e., $\tau_1' = 0$) and without decoupling during t_2, so that the observed cross peaks consist of doublets in antiphase with respect to $^1J(^{15}N,^1H)$ along ω_2. This modification of the experimental schemes requires that the phase Φ_4

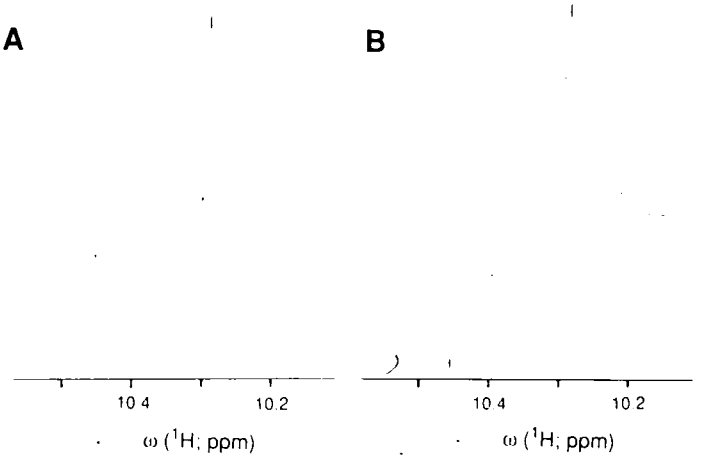

Fig. 2. Comparison of spin relaxation during τ_2 in the experiments of Figs. 1A and B, which select, respectively, single-quantum coherence or transverse two-spin coherence at the outset of τ_2. The measurements were made with the 434 repressor(1–69) at 13°C and the cross peak for the indole ring NH of Trp^{58} is shown. (A) Fourier transform of the first free induction decay of a J-modulated [^{15}N,^{1}H]-COSY spectrum recorded with the pulse sequence of Fig. 1A without ^{15}N refocusing pulse during τ_2, no decoupling during t_2, and with $\Phi_4 = [(y)_{16}(-y)_{16}]_2$ (Neri et al., 1990). (B) The same for the pulse sequence of Fig. 1B with $\tau_1' = 0$, no decoupling during t_2, and with $\Phi_4 = [(y)_{16}(-y)_{16}]_8$ (for both spectra: protein concentration 7 mM, $\tau_2 = 80$ ms, ^{1}H frequency 600 MHz on a Bruker AMX-600 spectrometer, processing and plotting with identical parameters).

is changed from $[(x)_{16}, (-x)_{16}]_n$ (Table 1) to $[(y)_{16}, (-y)_{16}]_n$ (Neri et al., 1990). Otherwise the two data sets were recorded and processed with identical conditions. Although the intensity of the high-field component of the antiphase doublets is practically the same in both spectra, the intensity of the low-field component is strongly reduced when the pulse sequence of Fig. 1A is used. This is due to the fact that the single-quantum coherence $\pm 2H_y^N N_z$ selected by the pulse sequence of Fig. 1A at the beginning of τ_2 is known to relax under the combined effects of dipolar coupling and chemical-shift anisotropy (Guéron et al., 1984; Goldman, 1984). In contrast, in macromolecules the transverse two-spin coherence, $2H_y^N N_y$, selected at the outset of τ_2 by the experiment B is to first order insensitive to heteronuclear dipolar coupling relaxation (Kay and Bax, 1990). Because the decoupled peaks obtained when using the complete experiments of Fig. 1 include the intensities of both fine-structure components (Fig. 2), significant improvements of the signal-to-noise ratio can be anticipated for the scheme B when compared with the scheme A, in particular for larger-size proteins for which dipolar relaxation makes a larger contribution to the overall relaxation rate.

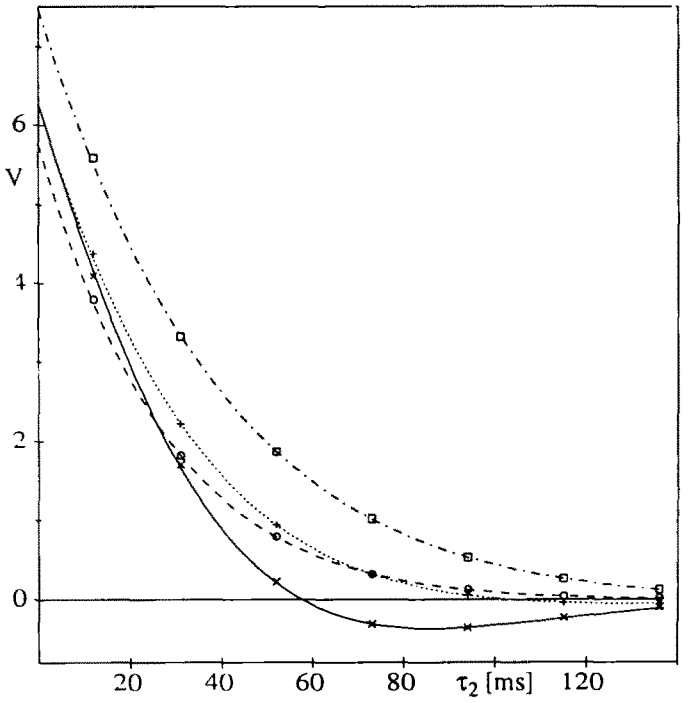

Fig. 3. Results of the fitting process of Eq. 7 for the 4 residues Gln^{17}, Ala^{21}, Thr^{27} and Leu^{34} of the 434 repressor(1–69). The cross-peak volumes are plotted vs. τ_2. A series of 7 J-modulated [^{15}N,^{1}H]-COSY spectra of a uniformly ^{15}N-labeled sample of the 434 repressor(1–69) was recorded with the τ_2 values indicated, using the experiment of Fig. 1B (protein concentration 7 mM, 99% ^{15}N-enrichment, solvent H_2O containing 25 mM K_2HPO_4 at pH 5.0, 100 mM KCl and 10% D_2O, T = 13°C, ^{1}H frequency 600 MHz on a Bruker AMX-600 spectrometer, data size 136 points in t_1 and 2048 points in t_2, t_{1max} = 54 ms, t_{2max} = 131 ms, total measuring time per experiment 12 h). Before Fourier transformation the time domain data were zero-filled to 512 points in t_1 and 4096 points in t_2 and multiplied with sine-bell windows along t_1 and t_2, with phase shifts of $\pi/5$ and $\pi/9$, respectively (De Marco and Wüthrich, 1976). The measured cross-peak volumes, V, and the fitted curve ($\bar{V}$ (τ_2) in Eq. 7) are indicated by × —— × for Thr^{27}, ○ - - - ○ for Gln^{17}, □ ·· –□ for Ala^{21}, and + ····· + for Leu^{34}.

Measurements of $^3J_{HN\alpha}$ in 434 repressor(1–69) at 13°C

The preparation of the uniformly ^{15}N-labeled 434 repressor(1–69) (M = 7.3 kDa) was described elsewhere (Anderson et al., 1984; Neri et al., 1989; Wider et al., 1989). Seven J-modulated [^{15}N,^1H]-COSY spectra at 13°C were recorded with the experiment of Fig. 1A (see Fig. 3 for experimental details). The individual values of the delay time τ_2 were distributed in regular intervals over the range 11–136 ms. Although the cross-peak volumes in the spectra recorded with short τ_2 delays are far from the point of sign inversion, τ_2^0, these data points are useful for the fit because they have the best signal-to-noise ratio and hence the smallest relative errors in the peak intensity measurements. With the conditions chosen for these experiments, i.e., an aqueous solution at 13°C, measurements of the $^3J_{HN\alpha}$ coupling constants with other methods are not straightforward even for a small protein, since the T_2 relaxation time is short and the lines are correspondingly broad. In the case of the 434 repressor(1–69) we found that for the well-structured protein segment 1–63, T_2' for amide protons is in the range 21–47 ms at 13°C. The same range of T_2' values was found for a protein–DNA complex with molecular weight 18 kDa in aqueous solution at 36°C (see below).

The Figs. 3 and 4 illustrate typical situations encountered in the data analysis. Figure 3 shows some of the nonlinear fits with Eq. 7 of the peak volumes measured for the 434 repressor(1–69) as a function of the delay time τ_2. These include residue Thr[27], which has a large coupling constant of 8.3 Hz, and Leu[34] with $^3J_{HN\alpha}$ = 4.8 Hz. For both residues a narrow error range was obtained (Table 2). For Thr[27], which has one of the largest χ^2_{min} values of all residues in the 434 repressor (1–69), this is due to the steep increase of $\chi^2(J)$ for values of J deviating from the optimal fit. For Leu[34] the very small value of χ^2_{min} contributes to the narrow error range, which is defined by intersecting the curve in Fig. 4 at a multiple of χ^2_{min}. Gln[17], with a coupling constant of 3.1 Hz, illustrates the situation where rapid T_2-relaxation, i.e., T_2' = 28 ms, dampens the signal intensity (Fig. 3). In spite of the strong asymmetry of the corresponding curve in Fig. 4, the lower limit, J_{ℓ}, is

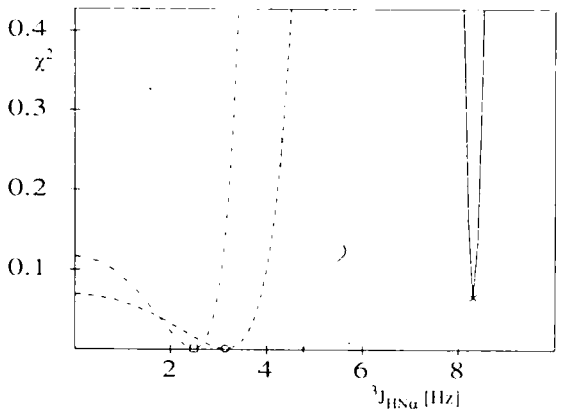

Fig. 4. Plot of the parameter χ^2 (Eq. 8) vs. $^3J_{HN\alpha}$ for the 434 repressor(1–69) at 13 C, with the range 0–10 Hz covered in steps of 0.1 Hz. These plots were obtained by first selecting an approximate value of $^3J_{HN\alpha}$, and then optimally fitting the two parameters A and T_2' with Eq. 7. Data are shown for the same 4 residues of the 434 repressor(1–69) as in Fig. 3: for Thr[27] (——), for Gln[17] (– – –), for Ala[21] (–·–·–) and for Leu[34] (·····). In the individual curves the optimal fit, with $\chi^2 = \chi^2_{min}$, is indicated by the symbols ×, +, o and □, respectively. In this presentation the extent of the vertical scale was chosen to be 5 times the average of χ^2_{min} of all residues for which $^3J_{HN\alpha}$ could be measured.

TABLE 2
PARAMETERS OBTAINED WITH THE FITTING PROCEDURES OF Eqs. 7 AND 8 USED TO EVALUATE THE $^3J_{HN\alpha}$ COUPLING CONSTANTS FOR THE 434 REPRESSOR(1–69) AT 13 C[a]

Residue[b]	$^3J_{HN\alpha}$ (Hz)	J_c (Hz)	J_u (Hz)	χ^2	A	T_2' (ms)
Ile[2]	2.4	2.3	2.5	< 0.01	4.4	28.6
Ser[3]	2.8	2.6	3.0	0.01	5.4	40.3
Ser[4]	4.8	4.7	4.8	0.01	5.3	38.3
Arg[5]	4.3	4.1	4.4	0.01	5.9	32.2
Val[6]	3.5	3.4	3.5	< 0.01	5.6	33.7
Lys[7]	2.9	2.7	3.0	0.01	7.1	36.5
Ser[8]	3.3	3.2	3.3	< 0.01	6.7	42.5
Lys[9]	4.6	4.5	4.6	< 0.01	4.7	35.0
Arg[10]	2.8	2.8	2.9	< 0.01	6.5	35.3
Ile[11]	4.9	4.8	5.0	0.01	4.6	35.1
Gln[12]	3.4	3.4	3.5	< 0.01	8.3	40.0
Leu[13]	6.1	6.1	6.2	0.01	7.8	36.1
Leu[15]	8.2	8.2	8.3	0.13	8.5	33.8
Asn[16]	7.9	7.8	8.1	0.01	4.6	24.4
Gln[17]	3.1	3.0	3.3	< 0.01	5.8	28.2
Ala[18]	4.3	4.2	4.3	< 0.01	3.7	42.7
Glu[19]	4.1	4.0	4.2	0.01	7.2	35.1
Leu[20]	4.0	3.9	4.1	0.01	7.8	33.1
Ala[21]	2.5	2.4	2.5	< 0.01	7.5	40.2
Gln[22]	3.7	3.7	3.8	0.01	8.4	44.9
Lys[23]	4.8	4.8	4.9	< 0.01	9.6	39.7
Val[24]	6.6	6.5	6.6	0.01	5.7	35.6
Thr[26]	8.4	8.3	8.5	0.35	6.5	40.6
Thr[27]	8.3	8.2	8.4	0.07	6.3	35.2
Gln[28]	1.9	1.7	2.1	< 0.01	5.8	33.7
Gln[29]	2.6	2.5	2.7	< 0.01	8.2	40.5
Ser[30]	4.2	4.2	4.3	< 0.01	5.8	37.5
Ile[31]	5.8	5.7	5.8	< 0.01	7.1	31.7
Glu[32]	2.9	2.9	3.0	< 0.01	5.2	36.8
Gln[33]	3.6	3.4	3.7	< 0.01	2.3	36.9
Leu[34]	4.8	4.7	4.8	< 0.01	6.3	34.3
Glu[35]	4.1	3.9	4.3	0.01	5.0	32.4
Asn[36]	7.1	7.1	7.2	0.02	5.4	32.4
Lys[38]	6.7	6.7	6.8	0.03	7.7	41.0
Thr[39]	8.2	8.1	8.2	0.36	8.1	42.8
Lys[40]	6.8	6.7	6.8	0.03	7.7	41.0
Arg[41]	7.8	7.8	7.9	0.78	10.2	40.6
Arg[43]	4.6	4.5	4.8	< 0.01	3.9	21.7
Leu[45]	2.9	2.3	3.3	< 0.01	4.6	23.3
Glu[47]	4.5	4.2	4.7	0.03	6.0	29.8
Leu[48]	4.1	4.0	4.2	0.01	5.7	31.7
Ala[49]	2.2	1.3	2.7	0.01	5.7	31.7
Ser[50]	3.6	3.6	3.7	< 0.01	9.2	46.6
Ala[51]	3.7	3.7	3.8	< 0.01	9.4	45.5
Leu[52]	7.1	7.1	7.2	< 0.01	3.0	33.3

TABLE 2 (*continued*)

Residue[b]	$^3J_{HN\alpha}$ (Hz)	J_o (Hz)	J_u (Hz)	χ^2	A	T'_2 (ms)
Val[54]	9.1	9.0	9.3	0.43	8.3	38.4
Ser[55]	6.5	6.4	6.6	0.03	5.2	33.1
Val[56]	3.5	3.4	3.5	< 0.01	7.6	33.1
Asp[57]	2.9	2.7	2.9	< 0.01	7.3	39.3
Trp[58]	4.0	3.8	4.1	0.01	4.4	34.3
Leu[59]	3.3	3.2	3.3	< 0.01	6.9	33.5
Asn[61]	8.8	8.8	8.9	0.10	6.0	36.9
Thr[63]	6.6	6.6	6.7	0.01	4.2	41.8
Ser[64]	6.4	6.3	6.4	0.14	11.3	54.3
Asp[65]	6.4	6.4	6.5	0.16	8.1	59.4
Ser[66]	6.4	6.3	6.4	0.03	12.4	80.3
Asn[67]	7.1	7.4	7.5	0.05	11.3	92.1
Val[68]	7.6	7.5	7.6	0.04	10.7	116.3
Arg[69]	7.4	7.4	7.5	0.03	11.1	106.2

[a] The experimental data measured as specified in Fig. 3 were fitted by Eq. 7 with the parameters $^3J_{HN\alpha}$, A and T'_2. The amplitude A is given in arbitrary units. J_o and J_u are lower and upper limits for $^3J_{HN\alpha}$ obtained from the $\chi^2(J)$ curves (Fig. 5) at the points where $\chi^2 = 2\chi^2_{min}$.

[b] Not listed are the glycyl residues 14, 25, 37, 53 and 62, prolyl 42 and 46, and the residues 44 and 60 for which the ^{15}N-^1H cross peaks were overlapped under the experimental conditions used (Fig. 3).

again quite precisely defined because of the very small value of χ^2_{min}. The fit for Ala[21], for which a $^3J_{HN\alpha}$ value of 2.5 Hz was obtained, is also associated with a very small χ^2_{min} value (Table 2 and Fig. 4). This can be rationalized by the fact that a good signal-to-noise ratio was obtained even for τ_2 = 136 ms, where the peak volume is still clearly positive (Fig. 3), showing that a significantly longer τ_2 delay than 136 ms would be needed for peak inversion. Following Eq. 1, $^3J_{HN\alpha}$ must therefore be very small.

Table 2 lists the $^3J_{HN\alpha}$ values obtained using the fit procedure of Eq. 7, as well as lower and upper error limits, J_o and J_u, which correspond to those values of $^3J_{HN\alpha}$ for which $\chi^2(J)$ is equal to twice the minimal value χ^2_{min} (Fig. 4). The remaining fit parameters A and T'_2 are also listed. In all, $^3J_{HN\alpha}$ determinations were obtained for 59 of the 69 residues in the 434 repressor(1–69). The 10 residues for which the data are missing are the N-terminus, 5 glycines, 2 prolines, and 2 residues for which the amide proton resonances were overlapped in the [^{15}N,^1H] plane (for details see Table 2).

With the cut-off of $\chi^2(J) = 2\chi^2_{min}$ chosen to define the error limits J_o and J_u in Table 2, practically all $^3J_{HN\alpha}$ values are well defined. The choice of this cut-off value for $\chi^2(J)$ was based on a systematic investigation of the influence of variable cut-off values on the error ranges obtained. In Fig. 5 the $^3J_{HN\alpha}$ values of Table 2 have been ordered by size along the horizontal axis. Error ranges obtained with a cut-off of $2\chi^2_{min}$ are plotted as dashed lines, and those for a cut-off of $5\chi^2_{min}$ as dotted lines. The figure shows that for most residues the choice of this factor was not critical. From Fig. 5 we further conclude that for small coupling constants, $^3J_{HN\alpha} < 3.0$ Hz, only an upper limit can be reliably derived with this method.

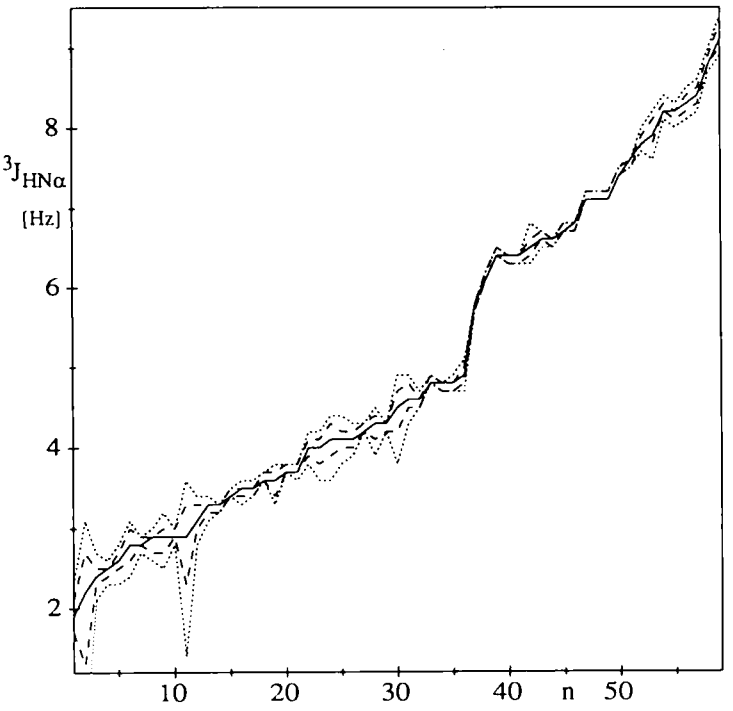

Fig. 5. Asymmetric error ranges for the values of $^3J_{HN\alpha}$ in the 434 repressor(1–69) at 13°C. In this presentation the coupling constants have been sorted along the horizontal axis according to increasing size; the index n is thus not related with the amino acid sequence. The error ranges have been calculated by reading the values of the lower and upper limits, J_ℓ and J_u, from curves of the type shown in Fig. 4. The solid line connects the values calculated for $^3J_{HN\alpha}$, the two broken lines represent the error limits obtained at $\chi^2(J) = 2\chi^2_{min}$ and the dotted lines those obtained at $\chi^2(J) = 5\chi^2_{min}$ (see text).

Measurements of $^3J_{HN\alpha}$ in a protein–DNA complex

The preparation of a 1:1 complex of the uniformly ^{15}N-labeled *Antennapedia* homeodomain with a 14-base pair DNA duplex was described in Otting et al. (1990). The molecular weight of this complex is ~18 kDa. A 0.5-mM solution of the complex was used at 36°C. As with the 434 repressor(1–69), a series of 7 J-modulated [^{15}N,^{1}H]-COSY spectra was recorded with the experimental scheme of Fig. 1B, but a shorter maximal delay τ_2 of 90 ms was used because with the 14-fold lower concentration, poor signal-to-noise ratios are implicated for longer τ_2-values. Each individual recording took about 9 h.

The measured cross-peak volumes and the fits with Eq. 7 are shown for selected residues in Fig. 6, and the χ^2 vs. J dependence for the same examples is presented in Fig. 7. The solid curves in these two figures describe the result obtained for Tyr^{25}, which has a large coupling constant of 8.2 Hz. The steep slopes of the plot of χ^2 as a function of J (Fig. 7) show that this coupling was determined with high precision. The values of J_ℓ and J_u for a cut-off of $2\chi^2_{min}$ are 8.1 and 8.3 Hz; they thus define an error range of $\pm$ 0.1 Hz. A measurement of a small coupling constant, 3.9 Hz, is given by the dash-dotted lines. The corresponding residue, Arg^{43}, is located in an α-helix (Qian et al., 1989). Although the lower limit, J_ℓ, is not precisely defined because of the small gradient of χ^2 vs. J in the left branch of the curve (Fig. 7), the upper limit is well defined by the steep increase of

the χ^2 vs. J curve. Tyr[11] (dotted curve) is also located in a helix (Qian et al., 1989) and has a small coupling of 4.6 Hz, but both an upper limit and a lower limit could be established. The fourth example (dashed curve) describes the residue Thr[27], which has a relaxation time T'_2 of 27.6 ms and is thus placed at the lower end of the observed range of T'_2 values for amide protons in this complex, which extends from 22 to 46 ms (the only exception is the C-terminal residue with a value of 90.3 ms). Figure 7 shows that in spite of the short relaxation time, the coupling constant of 7.7 Hz is well defined by the χ^2 vs. J curve.

Figure 8 presents the data on J, J_e and J_u obtained from Fig. 7 in the same way as in Fig. 5 above. With two exceptions all coupling constants larger than 4.5 Hz are determined within narrow limits. The exceptions are Arg[10] and Arg[28], which have small T'_2 values of 29.5 ms and 22.4 ms, respectively, and the smallest values for the cross-peak volume at time zero, A (Eq. 7). For couplings smaller than 4.5 Hz, no significant lower limit was usually obtained. The inability to obtain lower limits is probably due to the short maximal delay time τ_2 chosen for the experiments

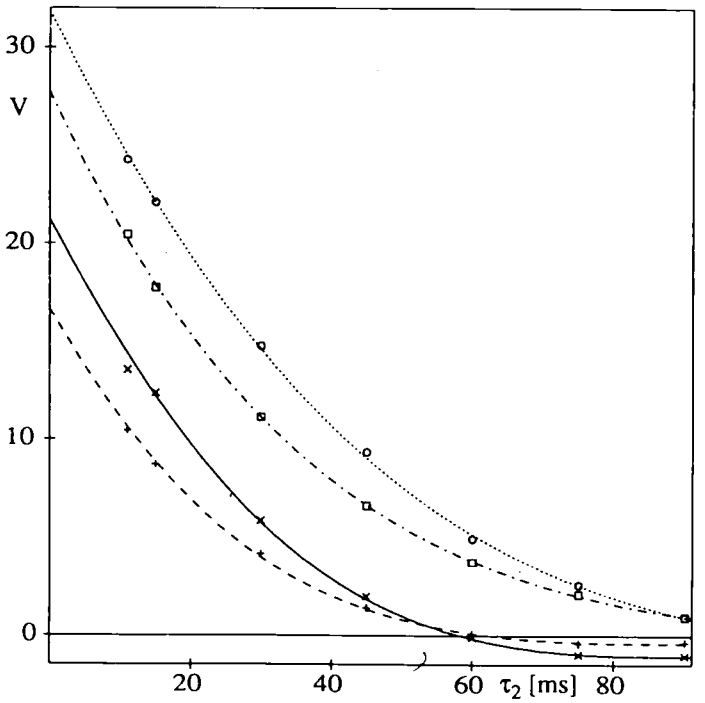

Fig. 6. Results of the fitting process of Eq. 7 for the 4 residues Tyr[11], Tyr[25], Thr[27] and Arg[43] of the *Antennapedia* homeodomain in a protein-DNA complex. The cross-peak volumes are plotted vs. τ_2. A series of 7 J-modulated [^{15}N,^{1}H]-COSY spectra of a uniformly ^{15}N-labeled sample of the *Antennapedia* homeodomain in a protein–DNA complex was recorded with the τ_2 values indicated, using the experiment of Fig. 1B (protein concentration 0.5 mM, 99% ^{15}N-enrichment, solvent H_2O containing 25 mM K_2HPO_4 at pH 6.0, 100 mM KCl and 6% D_2O, T = 36°C, ^{1}H frequency 600 MHz on a Bruker AM-600 spectrometer, data size 100 points in t_1 and 2048 points in t_2, $t_{1\,max}$ = 32 ms, $t_{2\,max}$ = 135 ms, total measuring time per experiment 9 h). Before Fourier transformation the time domain data were zero-filled to 512 points in t_1 and 4096 points in t_2 and multiplied with sine-bell windows along t_1 and t_2, with phase shifts of $\pi/3$ and $\pi/5$, respectively (De Marco and Wüthrich, 1976). The measured cross-peak volumes, V, and the fitted curve ($\overline{V}$ (τ_2) in Eq. 7) are indicated by × —— × for Tyr[25], +– – –+ for Thr[27], □–·–·–□ for Arg[43], and ○·····○ for Tyr[11].

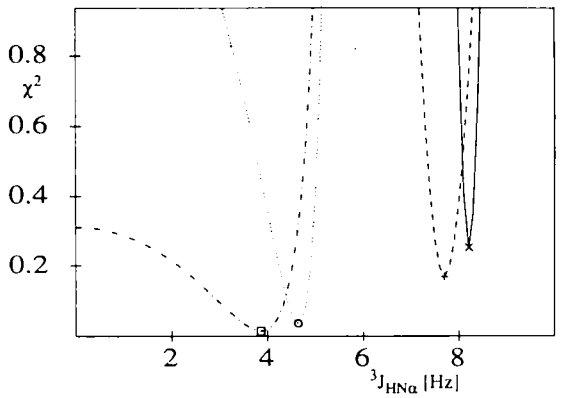

Fig. 7. Plot of the parameter χ^2 (Eq. 8) vs. $^3J_{HN\alpha}$ for the DNA-bound *Antennapedia* homeodomain, with the range 0–10 Hz covered in steps of 0.1 Hz. These plots were obtained by first selecting an approximate value of $^3J_{HN\alpha}$, and then optimally fitting the two parameters A and T_2' with Eq. 7. Data are shown for the same 4 residues of the *Antennapedia* homeodomain as in Fig. 6, using a solid line for Tyr^{25}, a dashed line for Thr^{27}, a dash-dotted line for Arg^{43}, and a dotted line for Tyr^{11}. In the individual curves the optimal fit, with $\chi^2 = \chi^2_{min}$, is indicated by the symbols ×, +, o and ⌴, respectively. The extent of the vertical scale was chosen as in Fig. 4.

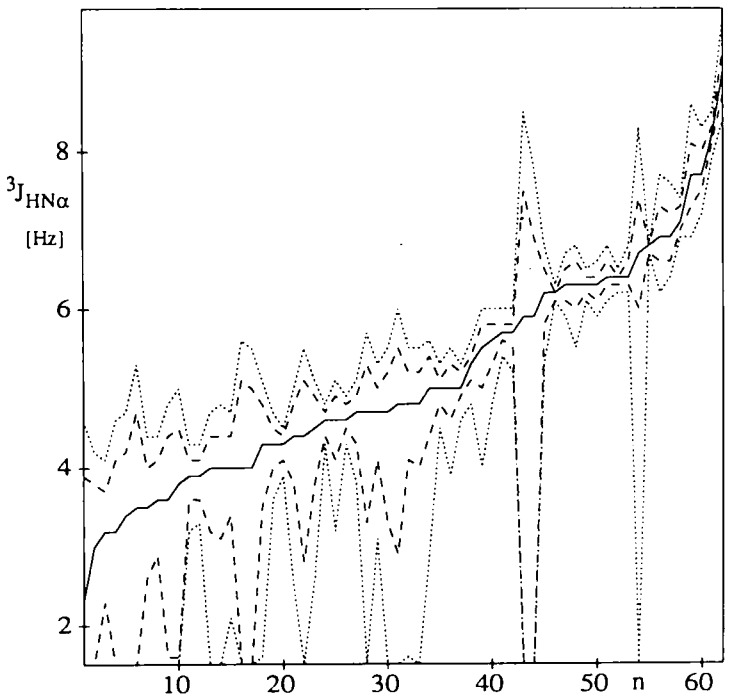

Fig. 8. Visual presentation of the asymmetric error ranges for the values of $^3J_{HN\alpha}$ in the *Antennapedia* homeodomain in a protein–DNA complex. In this presentation the coupling constants have been sorted along the horizontal axis according to increasing size, and n thus is an index that is unrelated with the amino acid sequence. The error ranges have been calculated by reading the values of the lower and upper limits, J_l and J_u, from curves of the type shown in Fig. 7. The solid line connects the values calculated for $^3J_{HN\alpha}$, the two broken lines represent the error limits obtained at $\chi^2(J) = 2\chi^2_{min}$ and the dotted lines those obtained at $\chi^2(J) = 5\chi^2_{min}$ (see text).

with this complex, whereas the choice of a maximal delay τ_2 of 136 ms for the 434 repressor(1–69) resulted in more precise data for small couplings. However, the structural information needed for the determination of the secondary structure is already contained in the measured upper limits for couplings smaller than about 5 Hz, or in the lower limits for couplings larger than about 7 Hz (Pardi et al., 1984). Most important, this information was readily obtained from the present experiments with a dilute solution of the complex. In Fig. 9 the J values of Fig. 8 are plotted vs. the protein sequence. A good correlation with the secondary structure of the protein (Qian et al., 1989; Otting et al., 1990) is readily apparent.

DISCUSSION

The two examples presented in Figs. 3–9 and Table 2 demonstrate that J-modulated [^{15}N,^{1}H]-COSY is capable of providing reliable data on $^{3}J_{HN\alpha}$ coupling constants in proteins under conditions which are generally known to make measurements of this parameter difficult. The method as described here provided the values for $^{3}J_{HN\alpha}$ that were used in the calculation of the structure of the 434 repressor(1–69) (Neri et al., 1992). Furthermore, the scalar couplings obtained with the J-modulated [^{15}N,^{1}H]-COSY experiment contributed direct evidence for the close structural similarity of the *Antennapedia* homeodomain in the free and complexed state (Otting et al., 1990). The

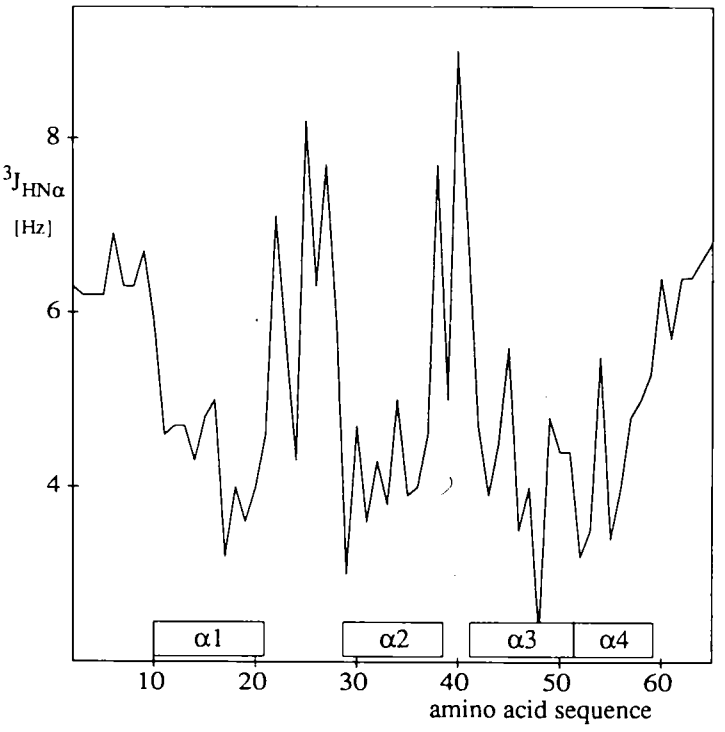

Fig. 9. Coupling constants $^{3}J_{HN\alpha}$ in the DNA-bound *Antennapedia* homeodomain plotted vs. the amino acid sequence. The location of the helices in the homeodomain (Qian et al., 1989; Otting et al., 1990) are indicated at the bottom with bars labeled α1–α4.

asymmetric uncertainty ranges illustrated by Figs. 5 and 8 and Table 2 are a special feature of the results obtained, which is further discussed in the following.

The values of χ^2_{min} obtained for the optimal fit of A, J and T'_2 in Eq. 7 show how well the experimental data can be fitted by the function given in Eq. 7. They are therefore also a good indication of the quality of the spectral data, i.e., they indicate to what extent the peak integrals are falsified by tails of neighboring peaks, or by noise, etc. For this reason we chose to base estimates of the error ranges on the χ^2_{min} values that were obtained for the optimal fits, and for each residue the error ranges given in Table 2 and Figs. 5 and 8 were defined by intersecting the $\chi^2(J)$ curve (Figs. 4 and 7) with a horizontal line at a given multiple of χ^2_{min}. In the application with the 434 repressor (1–69), variation of this multiplication factor between 2 and 5 did not critically influence the resulting error ranges, except for residues with large values of χ^2_{min}, which were then examined individually (Fig. 5).

The reason for the asymmetric distribution of J_o and J_u about the optimal value of J is the asymmetric shape of the curves in Figs. 4 and 7, which depend in a complex way on a large number of parameters. Among these parameters are the relaxation time T'_2 and A, the peak volume at $\tau_2 = 0$. Fast relaxation and a small initial peak volume will increase the average error in the peak integration and thus a larger selection of triplets of the fitting parameters A, J and T'_2 (Eq. 7) will give an acceptable fit with a low value of χ^2. Nearly symmetric curves are usually obtained for larger coupling constants, for which high-quality experimental data can be obtained.

ACKNOWLEDGEMENTS

Financial support by the Schweizerischer Nationalfonds (project 31.25174.88) is gratefully acknowledged. We thank D. Braun for providing us with home-made software routines for processing of 3D NMR data sets, Dr. G. Wider for discussions relating to 1D versions of the experiments of Fig. 1 (Weber et al., 1991), and R. Marani for the careful processing of the manuscript.

REFERENCES

Anderson, J., Ptashne, M. and Harrison, S.C. (1984) *Proc. Natl. Acad. Sci. USA*, **181**, 1307–1311.
Arseniev, A., Schultze, P., Wörgötter, E., Braun, W., Wagner, G., Vasak, M., Kägi, J.H.R. and Wüthrich, K. (1988) *J. Mol. Biol.*, **201**, 637–657.
Bodenhausen, G. and Ruben, D. (1980) *Chem. Phys. Lett.*, **69**, 185–188.
Bystrov, V.F. (1976) *Prog. NMR Spectrosc.*, **10**, 41–81.
De Marco, A. and Wüthrich, K. (1976) *J. Magn. Reson.*, **24**, 201–204.
De Marco, A., Llinás, M. and Wüthrich, K. (1978) *Biopolymers*, **17**, 637–650.
Eccles, C., Güntert, P., Billeter, M. and Wüthrich, K. (1991) *J. Biomol. NMR*, **1**, 111–130.
Goldman, M. (1984) *J. Magn. Reson.*, **60**, 437–452.
Guéron, M., Leroy, J.L. and Griffey, R.H. (1983) *J. Am. Chem. Soc.*, **105**, 7262–7266.
Güntert, P., Braun, W., Billeter, M. and Wüthrich, K. (1989) *J. Am. Chem. Soc.*, **111**, 3997–4004.
Karplus, M. (1959) *J. Phys. Chem.*, **30**, 11–15.
Karplus, M. (1963) *J. Am. Chem. Soc.*, **85**, 2870–2871.
Kay, L.E. and Bax, A. (1990) *J. Magn. Reson.*, **86**, 110–126.
Kay, L.E., Brooks, B., Sparks, S.W., Torchia, D.A. and Bax, A. (1989) *J. Am. Chem. Soc.*, **111**, 5488–5490.
Kim, Y. and Prestegard, J.H. (1989) *J. Magn. Reson.*, **84**, 9–13.
Ludvigsen, S., Andersen, K.V. and Poulsen, F.M. (1991) *J. Mol. Biol.*, **217**, 731–736.
McIntosh, L. and Dahlquist, F.W. (1990) *Quart. Rev. Biophys.*, **23**, 1–38.

Marion, D. and Wüthrich, K. (1983) *Biochem. Biophys. Res. Commun.*, **113**, 967–974.
Messerle, B.A., Wider, G., Otting, G., Weber, C. and Wüthrich, K. (1989) *J. Magn. Reson.*, **85**, 608–613.
Montelione, G. and Wagner, G. (1989) *J. Am. Chem. Soc.*, **111**, 5474–5475.
Nagayama, K. and Wüthrich, K. (1981) *Eur. J. Biochem.*, **115**, 653–657.
Neri, D., Szyperski, T., Otting, G., Senn, H. and Wüthrich, K. (1989) *Biochemistry*, **28**, 7510–7516.
Neri, D., Otting, G. and Wüthrich, K. (1990) *J. Am. Chem. Soc.*, **112**, 3663–3665.
Neri, D., Billeter, M. and Wüthrich, K. (1992) *J. Mol. Biol.*, **223**, 743–767.
Neuhaus, D., Wagner, G., Vasak, M., Kägi, J.H.R. and Wüthrich, K. (1985) *Eur. J. Biochem.*, **151**, 257–273.
Otting, G. and Wüthrich, K. (1988) *J. Magn. Reson.*, **76**, 569–574.
Otting, G. and Wüthrich, K. (1990) *Quart. Rev. Biophys.*, **23**, 39–96.
Otting, G., Qian, Y.Q., Billeter, M., Müller, M., Affolter, M., Gehring, W.J. and Wüthrich, K. (1990) *EMBO J.*, **9**, 3085–3092.
Pardi, A., Billeter, M. and Wüthrich, K. (1984) *J. Mol. Biol.*, **180**, 741–751.
Press, W.M., Flannery, B.P., Teukolsky, S.A. and Vetterling, W.T. (1986) *Numerical Recipes*, Cambridge University Press, Cambridge.
Qian, Y.Q., Billeter, M., Otting, G., Müller, M., Gehring, W.J. and Wüthrich, K. (1989) *Cell*, **59**, 573–580.
Shaka, A.J., Barker, P.B., Bauer, C.J. and Freeman, R. (1986) *J. Magn. Reson.*, **67**, 396–401.
Sørensen, O.W., Eich, G.W., Levitt, M.H., Bodenhausen, G. and Ernst, R.R. (1983) *Prog. NMR Spectrosc.*, **16**, 163–192.
Wagner, G., Schmieder, P. and Thanabal, V. (1991) *J. Magn. Reson.*, **93**, 436–440.
Weber, C., Wider, G., von Freyberg, B., Traber, R., Braun, W., Widmer, H. and Wüthrich, K. (1991) *Biochemistry*, **30**, 6563–6574.
Wider, G., Neri, D., Otting, G. and Wüthrich, K. (1989) *J. Magn. Reson.*, **83**, 426–431.
Wüthrich, K. (1986) *NMR of Proteins and Nucleic Acids*, Wiley, New York.
Wüthrich, K. (1990) *J. Biol. Chem.*, **265**, 22059–22062.